Hindawi
Shock and Vibration
Volume 2024, Article ID 9235312, 12 pages
https://doi.org/10.1155/2024/9235312

Research Article

Numerical Investigation on the Flow Field of Muzzle Decompression Device for the Barrel Recoil Gun

Zilong Liu,[1] Jinsong Dai,[1] Shengye Lin,[1] Dong Zhou,[2] Maosen Wang,[1] and Haifeng Wang[3]

[1]*The School of Mechanical Engineering, Nanjing University of Science and Technology, Nanjing, Jiangsu 210094, China*
[2]*Shenyang Aircraft Design and Research Institute, Shenyang, Liaoning 110035, China*
[3]*Xi'an Kunlun Industrial Group Co., Ltd., Xi'an, Shaanxi 710043, China*

Correspondence should be addressed to Jinsong Dai; djs101@163.com

Received 2 November 2023; Revised 7 March 2024; Accepted 15 March 2024; Published 22 March 2024

Academic Editor: Antonio Giuffrida

A structured dynamic overlapping grid and a user-defined function are used to study the projectile launching process, and the hybrid Roe scheme is used to solve the flow field with strong shock wave. The launching process of a projectile with a muzzle decompression device is numerically simulated by using a three-dimensional transient model, and the flow field inside the muzzle decompression device and the development process of the muzzle flow field in the projectile launching process are discussed in detail. Compared with no device, the muzzle decompression device can effectively reduce the peak pressure around the muzzle; the numerical results are in agreement with the corresponding experimental values. The numerical investigation in this paper is helpful to understand the mechanism of pressure reduction of the device. It also provides a new way to reduce the muzzle pressure of aircraft gun.

1. Introduction

The transient flow field with strong shock wave formed after gun firing is very complicated. The muzzle flow field usually consists of two shock waves. The first is caused by the projectile starting to accelerate in the barrel, which pushes and compressions the air column in front of it to produce a shock wave and then diffraction occurs at the muzzle. The second is caused by the projectile flying away from the muzzle, and the high-temperature and high-pressure propellant gas is expelled and expanded instantaneously. For warplanes, muzzle shock wave will cause a sudden increase in pressure around the muzzle, which is easy to cause vibration of the aircraft body around the muzzle, thus affecting the normal operation of airborne equipment and even causing damage in serious cases. Therefore, in order to reduce the peak pressure of muzzle flow field, it is necessary to investigate the muzzle decompression device.

In the past few decades, a series of theoretical research, experiments, and numerical simulation have been carried out on muzzle flow field [1–3]. Li et al. [4, 5] studied the evolution process of supersonic muzzle jet based on dynamic mesh technology, and the results showed that the muzzle jet distorts under the influence of constrained boundary. The effects of different projectile velocities and shapes on the muzzle flow field were studied in [6, 7]. In addition, the combustion mechanism of chemical reaction is gradually applied to the study of the muzzle flow field. Sun et al. [8–13] studied the shock wave and jet and secondary combustion processes in the muzzle flow field by numerical simulation using detailed chemical reaction dynamics models. In the visualization of the muzzle flow field, Moumen [14, 15] combined Schlieren technology with high-speed cameras to realize quantitative visualization of traffic, and the results showed that this technique could visualize the density flow field. In the measurement of muzzle shock wave pressure, Kong et al. [16, 17] used a piezoelectric sensor to measure the muzzle overpressure and established the distribution law of the muzzle overpressure.

Due to the high temperature, high pressure, and high speed of the propellant gas at the muzzle, thus has great harmfulness, some scholars have studied various hazards

caused by the muzzle flow field. Zhao [18] used the method of numerical simulation and experiment to study the noise produced by small-caliber rifle shooting and analyzed the distribution rule of noise produced by jet. Ding [19] calculated the value of the overpressure generated by the firing of the aircraft gun, established the expression of the impact load, and calculated the dynamic response of the aircraft cabin under the load.

Previous studies have been very perfect in revealing the formation, development, and distribution of muzzle shock waves, and the test methods are very mature. At present, most studies on the harm of shock wave overpressure focus on the distribution of overpressure value in different scenarios, and the measures to reduce overpressure value are rarely proposed. In this paper, a muzzle device which can reduce the muzzle overpressure value is designed for small-caliber aircraft gun. The working principle of the device is revealed by numerical simulation and verified by experiment. The research results are of great significance for understanding the muzzle flow field characteristics and designing the muzzle decompression device.

2. Model and Method

2.1. Design of the Parameter Scheme. Figure 1 shows the computational domain inside the muzzle decompression device; there are 6 holes evenly distributed on the inner wall and the front wall. The computational domain of the whole numerical simulation and the corresponding boundary conditions are shown in Figure 2, and the length of the barrel is $L2 = 1.5m$, the radius of the barrel is $R2 = 0.015m$ (the radius of the projectile is also 0.015m), and the length of the projectile is $L3 = 0.1m$. The boundary condition of the wall of the barrel, projectile, and muzzle depression device is defined as "wall," the outer boundary of the projectile is defined as "overset," and the boundary condition of the outside domain is "pressure outlet."

2.2. Model Establishment and Mesh Division. In this paper, the dynamic overlapping grid method is used for numerical simulation. The mesh system of the muzzle flow field established in this paper consists of two parts, a component grid describing the high-speed moving projectile and a static background grid describing the environment around the barrel and muzzle decompression device. In order to ensure the simulation accuracy, structural mesh is used, and the density of the grid around the trajectory of projectile is improved. Figure 3 shows the grid model; after grid convergence testing, the background grid of the computational domain has a total of 2,530,000 cells and the component grid has a total of 96,000 cells. The standard K-Epsilon turbulence two-equation model calculates the whole flow field in this simulation; the model is commonly used to calculate turbulent flow with high Reynolds number and has the advantages of moderate computation, easy convergence, and considerable computational accuracy, and its expression is as follows:

$$\begin{aligned}\frac{\partial}{\partial t}(\rho k)+\frac{\partial}{\partial x_i}(\rho \mathrm{ku}_i)&=\frac{\partial}{\partial x_j}\left[\left(\mu+\frac{\mu_t}{\sigma_k}\right)\frac{\partial k}{\partial x_j}\right]-\rho\overline{\mu_i'\mu_j'}\frac{\partial \mu_j}{\partial x_i}-\rho\varepsilon,\\ \frac{\partial}{\partial t}(\rho\varepsilon)+\frac{\partial}{\partial x_i}(\rho\varepsilon u_i)&=\frac{\partial}{\partial x_j}\left[\left(\mu+\frac{\mu_t}{\sigma_\varepsilon}\right)\frac{\partial \varepsilon}{\partial x_j}\right]-C_{\varepsilon 2}\rho\frac{\varepsilon^2}{k}+C_{\varepsilon 1}\frac{\varepsilon}{k}\rho\overline{\mu_i'\mu_j'}\frac{\partial \mu_j}{\partial x_i}.\end{aligned} \tag{1}$$

In the equation, ρ is the gas density, k is the turbulent kinetic energy, and ε is the turbulent diffusivity. u_i and u_j are velocity components and $\overline{\mu_i'\mu_j'}$ is the Reynolds pressure term. σ_k and σ_ε are the Prandtl number for the turbulent kinetic energy and the dissipation rate, respectively. In this case, $\sigma_k = 1.0$ and $\sigma_\varepsilon = 1.3$; $\mu_t = C_\mu k^2/\varepsilon$ is the turbulent viscosity; and the constants $C_{\varepsilon 1} = 1.44$, $C_{\varepsilon 2} = 1.92$, and $C_\mu = 0.09$ represent the empirical coefficients.

In the numerical simulation, the convergence accuracy is set to 10^{-5}, the time step is set to $10^{-6}s$, and the number of time steps is 2000. The required convergence accuracy can be achieved. The numerical simulation is divided into two stages as follows: first, the projectile is placed at the bottom of the barrel and gradually begins to accelerate, where the precursor shock wave is formed. Before the projectile moves, the pressure in the area in front of the projectile was set to 101325 Pa, the temperature to 300 K, and the gas velocity to 0 m/s. The velocity of the projectile is calculated by the internal ballistic model; when the projectile is about to fly away from the muzzle, its velocity is 860 m/s. The numerical simulation enters the second stage. When the projectile bottom is about to pass the muzzle, we set the gas temperature in the barrel as 1800 K, the propellant gas pressure at the projectile bottom as 60 MPa, and the velocity as 860 m/s. The gas parameters in the barrel are calculated by the mathematical model of internal ballistic gas dynamics; considering the propellant gas as a homogeneous flow, the equations of continuity and motion are as follows:

$$\begin{aligned}\frac{\partial \rho}{\partial t}+\frac{\partial(\rho v_x)}{\partial x}&=0,\\ \frac{\partial v_x}{\partial t}+v_x\frac{\partial v_x}{\partial x}&=-\frac{1}{\rho}\frac{\partial p_x}{\partial x},\end{aligned} \tag{2}$$

where x is the distance between the bottom of the barrel and the projectile, t is the time variable, ρ is the gas density, and v_x is gas velocity in the barrel.

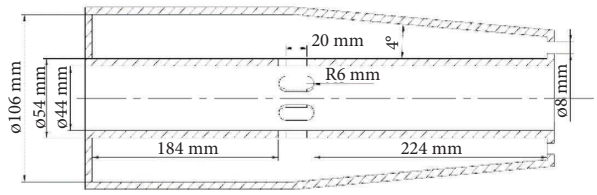

Figure 1: Computational domain of the muzzle decompression device.

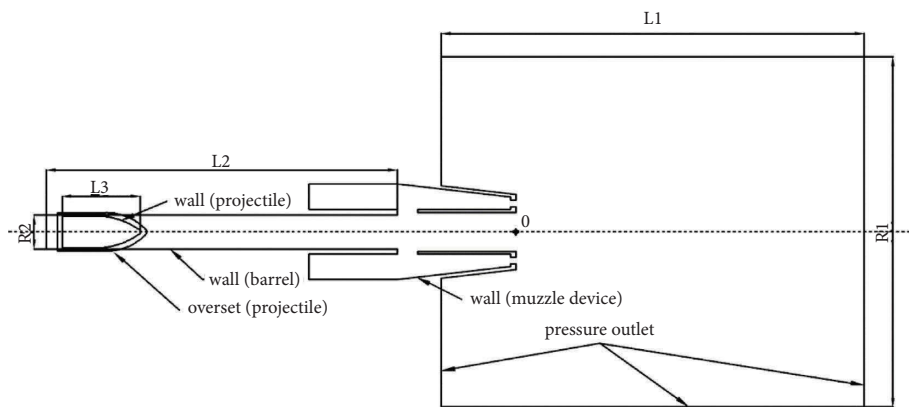

Figure 2: Computational domain and boundary conditions.

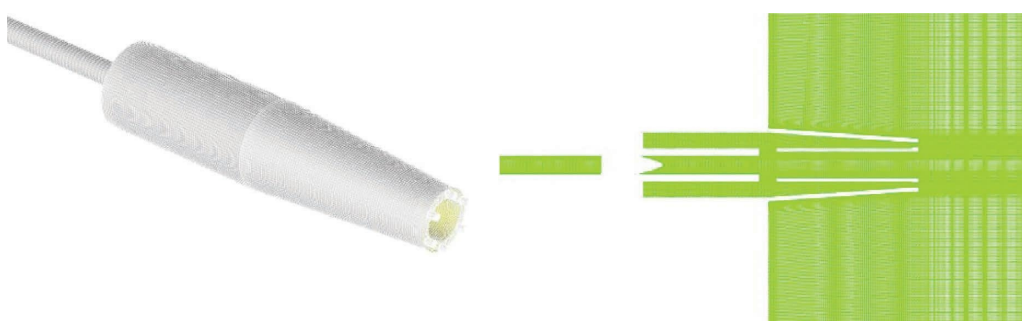

(a) (b)

Figure 3: Grid model. (a) Mesh of device. (b) Mesh of the computational domain.

Using the Lagrange assumption that the gas density in the barrel is uniformly distributed, the following formula can be obtained:

$$\left(\frac{\partial \rho}{\partial x}\right) = 0. \tag{3}$$

Equation of projectile motion is as follows:

$$\frac{\mathrm{dv}}{\mathrm{dt}} = \frac{A}{\varphi m} p_d, \tag{4}$$

where v is the projectile velocity, A the sectional area of the projectile, m is the projectile mass, φ is the secondary work coefficient, and p_d is the gas pressure at the bottom of the projectile.

The propellant gas pressure and velocity inside the barrel are obtained from the boundary conditions, where $v_x = 0$ for $x = 0$, $v_x = v$ for $x = L$, and $p_x = p_d$ for $x = L$:

$$\begin{aligned} p_x &= p_d\left[1 + \frac{\omega}{2\varphi m}\left(1 - \frac{x^2}{L^2}\right)\right] \\ v_x &= \frac{x}{L} v, \end{aligned} \tag{5}$$

where ω is the propellant mass, p_x is the gas pressure in the barrel, L is the length of the barrel, and $\omega/2\varphi m = 0.12$.

2.3. Experimental System. Ground firing experiment was carried out to verify the numerical simulation model and to better study the effect of the muzzle decompression device. The overpressure is measured using the pressure sensor type 211B3 from KISTLER, Switzerland, which has a measuring range of 500 psi. As shown in Figure 4(a), the corresponding experimental system is composed of the following three parts: launch platform, 30 mm caliber aircraft gun, and

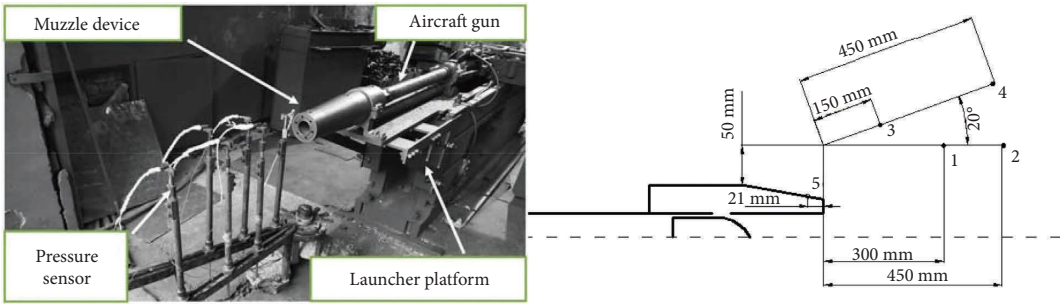

(a) (b)

Figure 4: Experimental system. (a) Experimental facility. (b) Sensor location.

pressure measurement system. The launch platform is fixed on the cement platform, above which is installed a 30 mm caliber aircraft gun; muzzle decompression device is also fixed on the launch platform, and the overpressure around the muzzle is measured by pressure sensor and recorded by computer. The sensors are arranged as shown in Figure 4(b). During the test, the gun was fired without device and the muzzle overpressure data were collected. Then, the device was mounted on the launch platform, and the pressure sensor was moved 256 mm along the muzzle to ensure that the relative position of the test point remained unchanged, fired again, and collected overpressure data.

3. Results and Discussion

3.1. Numerical Simulation and Experimental Verification without Muzzle Decompression Device. In order to verify the reliability of the numerical simulation model in this paper and the depressurization efficiency of the device, numerical simulation was conducted for the scene without the muzzle depressurization device. Each simulation condition is the same as that with the decompression device, and the time of the projectile coming out of the muzzle is defined as $t = 0$, and the results are as follows.

Figure 5 shows part of the muzzle flow field development process without muzzle decompression device. When the projectile accelerates in the barrel, it pushes and compresses the air column in front of the projectile, thus a series of compression waves are formed and gradually forming a shock wave front with the movement of the projectile, which is the precursor shock wave, as shown in Figures 5(a)–5(c). Figure 5(d) shows that as the projectile flies away from the barrel, the precursor shock wave continues to expand into a sphere, and the high-pressure gas rushes out of the barrel at a higher speed than the precursor shock wave and the projectile. After chasing and overtaking the projectile, the gas travels forward along the side wall of the projectile. It can be seen from Figures 5(e) and 5(f) that when the projectile penetrates the precursor shock wave, since the motion of the projectile with respect to the gas in front is supersonic, a high-intensity bow shock is formed at the head of the projectile.

In the process of numerical simulation, the pressure monitoring of several points around the muzzle is carried out, and the position of each monitoring point is the same as that of the pressure sensor in the experiment. Figure 6 shows the pressure change at each monitoring point. It can be seen that the pressure value at each monitoring point increases sharply after the propellant gas rushed from the barrel. The monitoring point 3 closest to the muzzle was the first to be impacted by gas, and its peak pressure reached 3.21 MPa. With the position of the monitoring point gradually away from the muzzle, the peak value of other monitoring points decreased significantly. Since monitoring points 2 and 4 are almost the same distance from the center of the muzzle, the shock waves of the time and intensity are relatively close to arrive here.

Table 1 shows the peak pressure measured by the ground firing test of the aircraft gun without the muzzle decompression device. It can be seen that the maximum pressure measured by the numerical results is basically consistent with that measured by the experiment, and the maximum error is 9.6%, which indicates that the numerical simulation in this paper is credible.

3.2. Numerical Simulation and Experimental Verification with Muzzle Decompression Device. Figure 7 shows the evolution of the muzzle flow field with muzzle decompression device. It can be seen from Figures 7(a) and 7(b) that the precursor shock wave formed by the air column in front of the projectile is destroyed by the device and part of the high-pressure gas in front of the projectile enters the chamber of the device. When the projectile flies off the barrel, part of the high-pressure propellant gas in barrel quickly flows into the chamber through the hole on the inner wall of the muzzle decompression device. Figure 7(c) shows that after the propellant gas impacts the wall of the device, it expands forward and backward. As shown in Figure 7(d), since the inner diameter of the muzzle decompression device is much larger than the diameter of the projectile, the propelling gas behind the projectile starts to chase and overtake the projectile before it leaves the device, and when the projectile flies off the decompression device, the precursor shock wave formed in front of the projectile contains not only the compressed column of air in front of the projectile but also part of the high-pressure propelled gas. It can be seen from Figures 7(e) and 7(g) that propellant gas is gradually ejected from the nozzle decompression device after the projectile flies away. At the

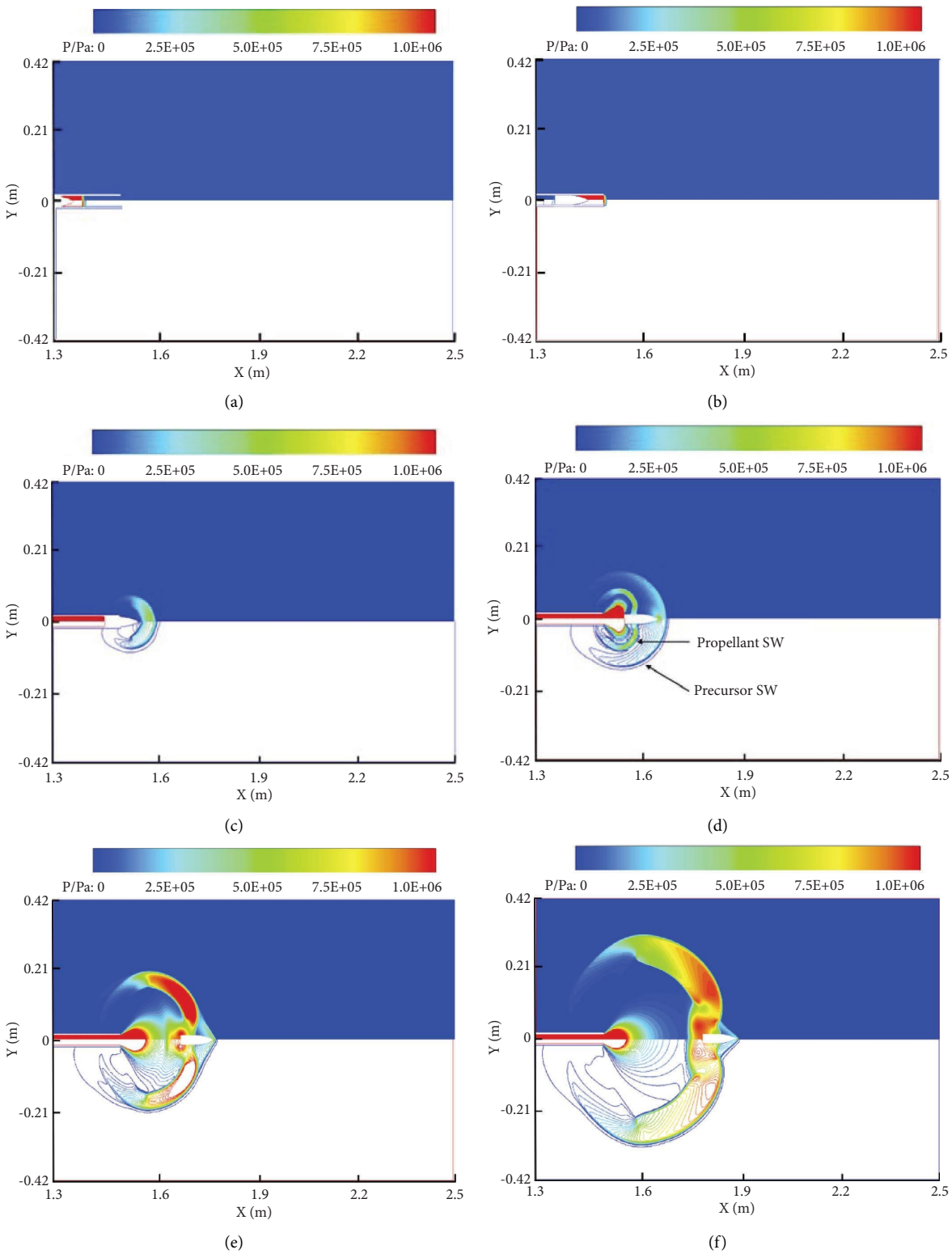

Figure 5: Pressure contours of the muzzle flow. (a) $t = -0.25$ ms. (b) $t = -0.15$ ms. (c) $t = -0.05$ ms. (d) $t = 0.05$ ms. (e) $t = 0.15$ ms. (f) $t = 0.25$ ms.

same time, more propellant gas enters the chamber, raising the pressure inside the chamber and then ejected through small holes at the front of the muzzle decompression device. Figure 7(h) shows that as the projectile moves gradually, the bottom shock wave forms, the presence of the projectile prevents the formation of the Mach disk, and the shock wave formed by the propellant gas expands into a larger sphere.

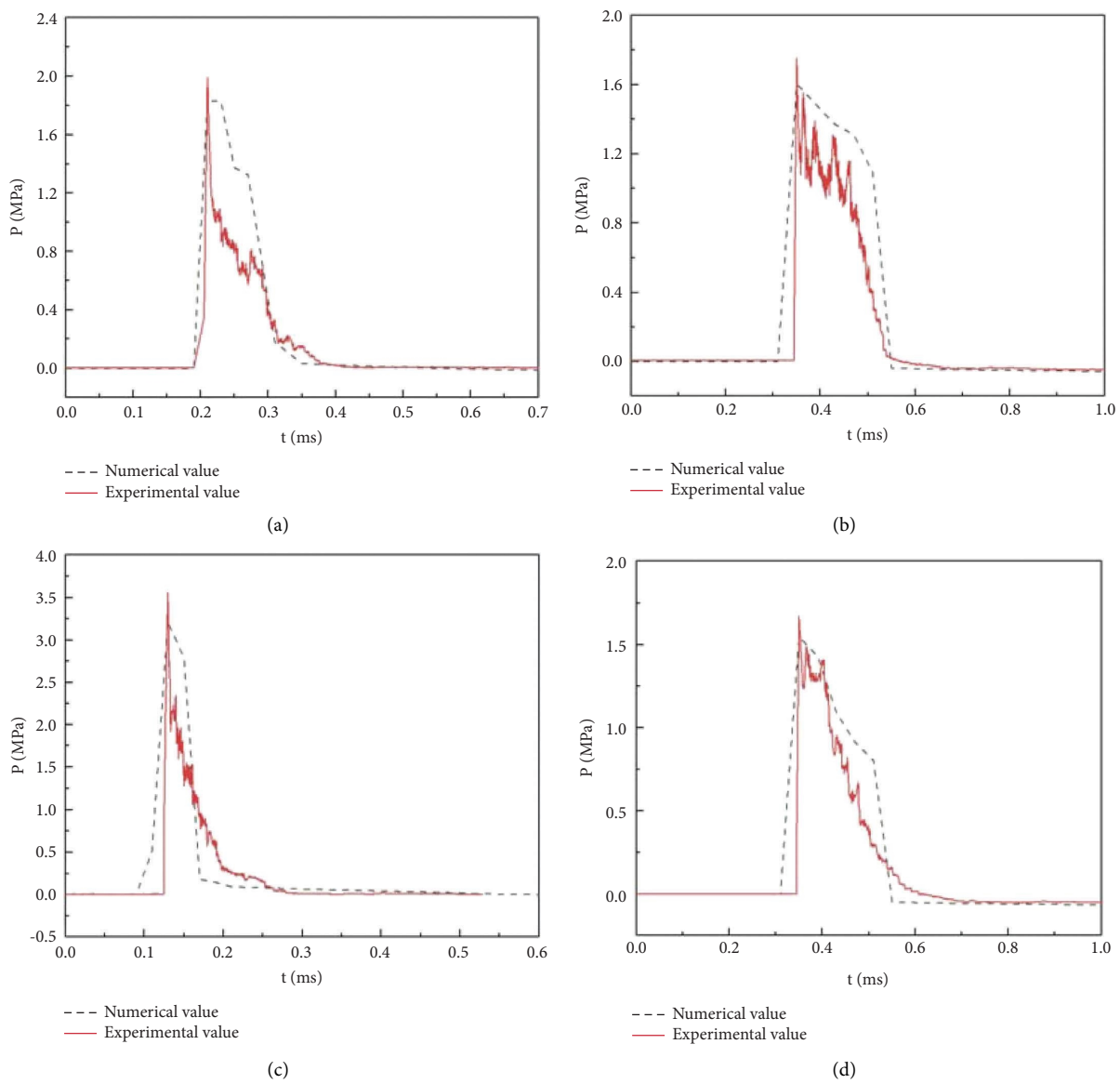

Figure 6: Pressure curve at monitoring points without device.

Table 1: Peak pressure at the monitoring points without device.

Serial number	Numerical value (MPa)	Experimental value (MPa)	Error (%)
1	1.83	1.99	8.0
2	1.60	1.75	8.6
3	3.21	3.55	9.6
4	1.55	1.67	7.2

Figure 8 shows the Mach number contours of the muzzle flow field with muzzle decompression device. After the projectile passed the muzzle, the expansion process of high-pressure propellant gas at the muzzle creates Prandtl–Meyer (PM) expansion waves, and the expansion waves spread radially at high speeds, but limited by the wall of the decompression device and reflected after hitting the wall, and then transformed into a compression wave. During the motion of the propellant gas, these compression waves merge into shock waves surrounding the core of the propellant gas jet. As the compression wave gets closer to the center of the gas jet, its direction of motion is gradually parallel to the jet axis, thus forming a shock wave perpendicular to the jet axis, which is Mach disk. After the supersonic propellant gas passes through the Mach disk, the pressure increases and the velocity decreases to subsonic. At this point, the propellant gas is still in the state of high pressure; the gas will expand again and form expansion waves and then the previous process will be repeated until the

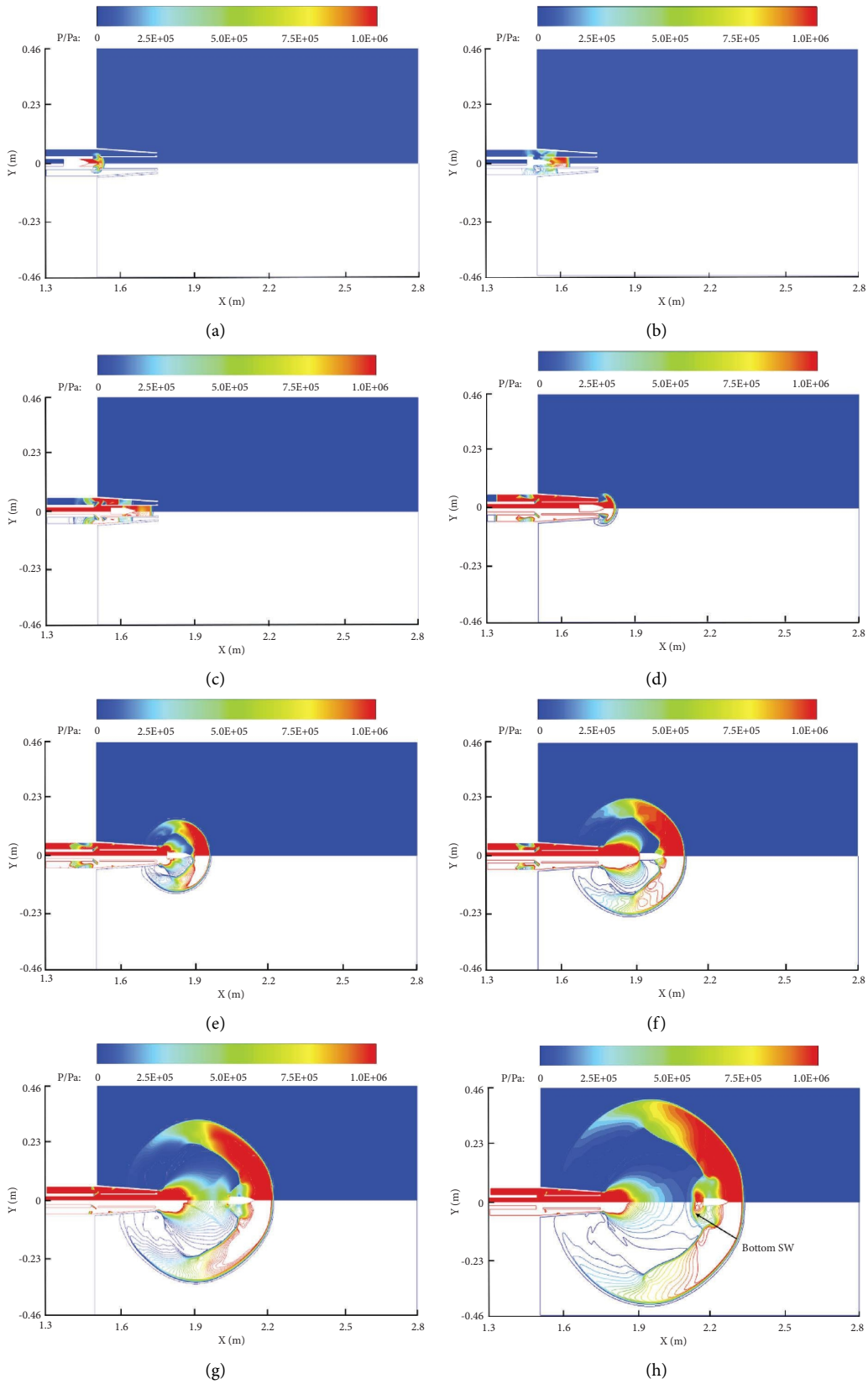

Figure 7: Pressure contour of the muzzle flow field of muzzle decompression device. (a) $t = -0.16$ ms. (b) $t = -0.06$ ms. (c) $t = 0.06$ ms. (d) $t = 0.16$ ms. (e) $t = 0.26$ ms. (f) $t = 0.36$ ms. (g) $t = 0.46$ ms. (h) $t = 0.56$ ms.

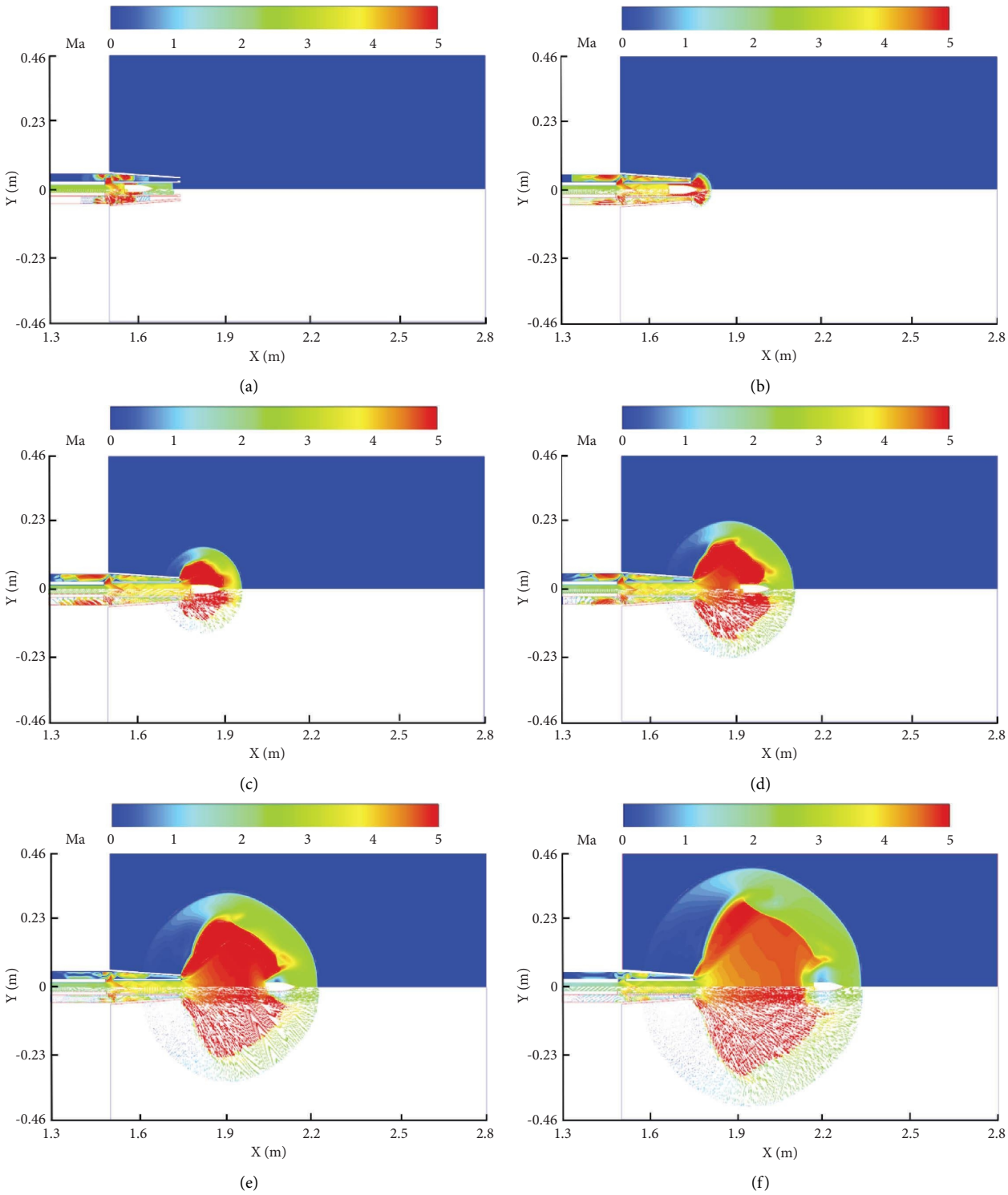

Figure 8: Pressure contour of the muzzle flow field of muzzle decompression device. (a) $t = 0.06$ ms. (b) $t = 0.16$ ms. (c) $t = 0.26$ ms. (d) $t = 0.36$ ms. (e) $t = 0.46$ ms. (f) $t = 0.56$ ms.

energy is dissipated so that no shock wave can be formed. Three shock wave units inside the device can be seen clearly in Figures 8(b)–8(d).

Figure 9 shows the pressure curve of each monitoring point with or without muzzle decompression device. The increase of projectile travel after the installation of the muzzle decompression device delays the impact time of the monitoring point; the peak pressure was decreased by 40.0% at monitoring points 3 and 4, by 25.0% at monitoring point 2, while had no significant change at monitoring point 1. By comparison, it can be found that with the increase of axial and radial distance between the monitoring point and the

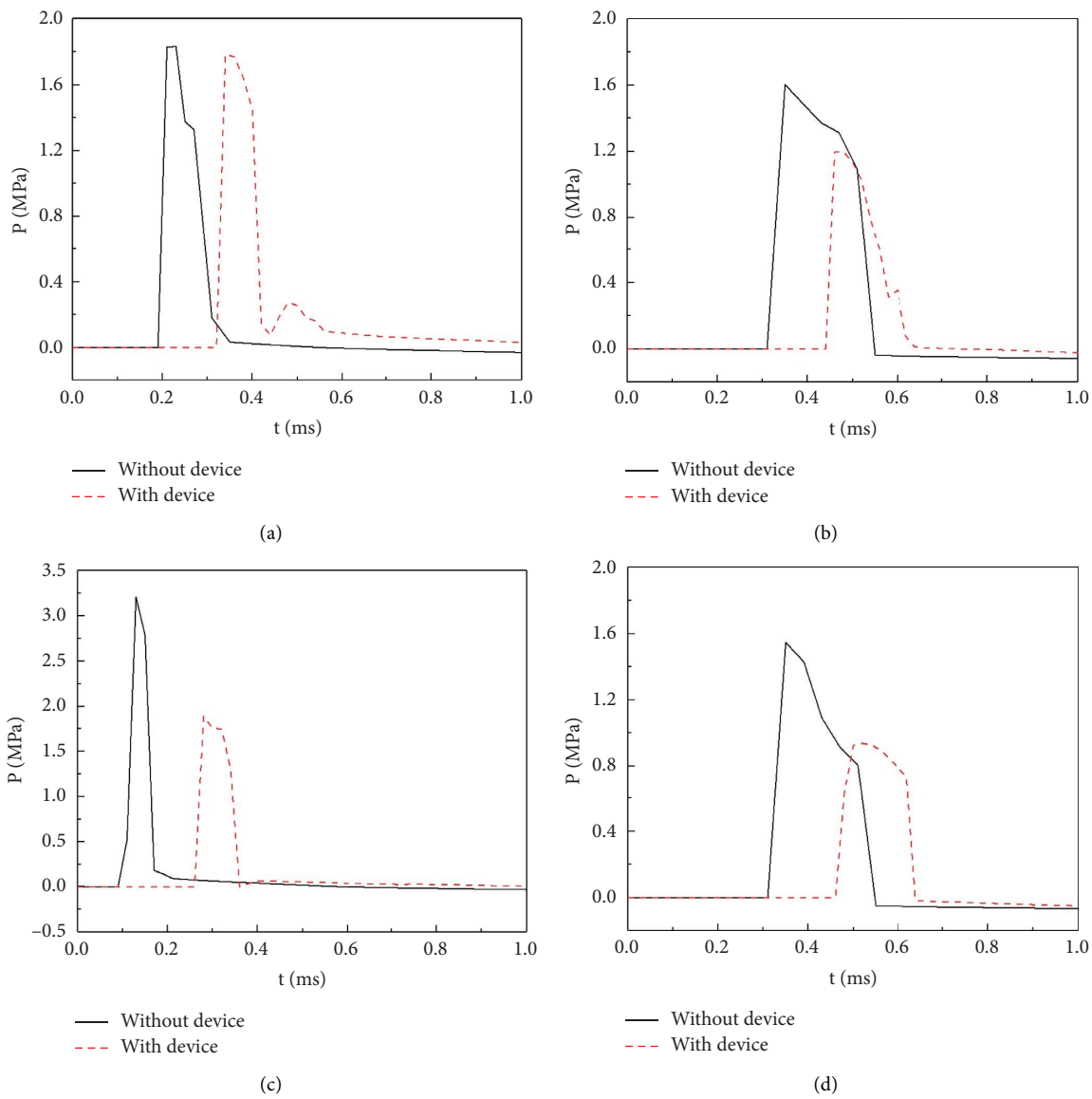

Figure 9: Comparison of pressure curve at monitoring points.

barrel axis, the peak pressure of the monitoring point with the muzzle decompression device decreased more than that without the device.

Figure 10 and Table 2 show the dynamic pressure curve and peak pressure measured by the ground firing test of the aircraft gun with a decompression device. It can be seen that the peak pressure measured by the numerical results is basically consistent with that measured by the test, and the maximum error is 9.3%, which verifies the correctness of the numerical model in this paper.

Figure 11 shows the changes of axial force and velocity of the projectile after it flies away from the barrel under two working conditions. As can be seen from the figure, after the projectile flies away from the body tube, it continues to accelerate under the action of high-pressure propellant gas inside the device, and the velocity of the projectile is finally increased by 7 m/s compared with that without the device.

When the projectile moves inside the device, it will have a certain influence on the movement of the gas inside the barrel. As shown in Figure 12, since the velocity of the projectile is lower than that of the high-pressure propellant gas, its movement in the device will limit the movement of the gas behind the projectile. As a result, the gas pressure drop speed at the center of the muzzle decreases and the gas velocity drop increases compared with that without the device. When the projectile flies away from the device, the gas pressure at the center of the muzzle increases by 1.9% and the gas velocity decreases by 1.2% compared with that without the device.

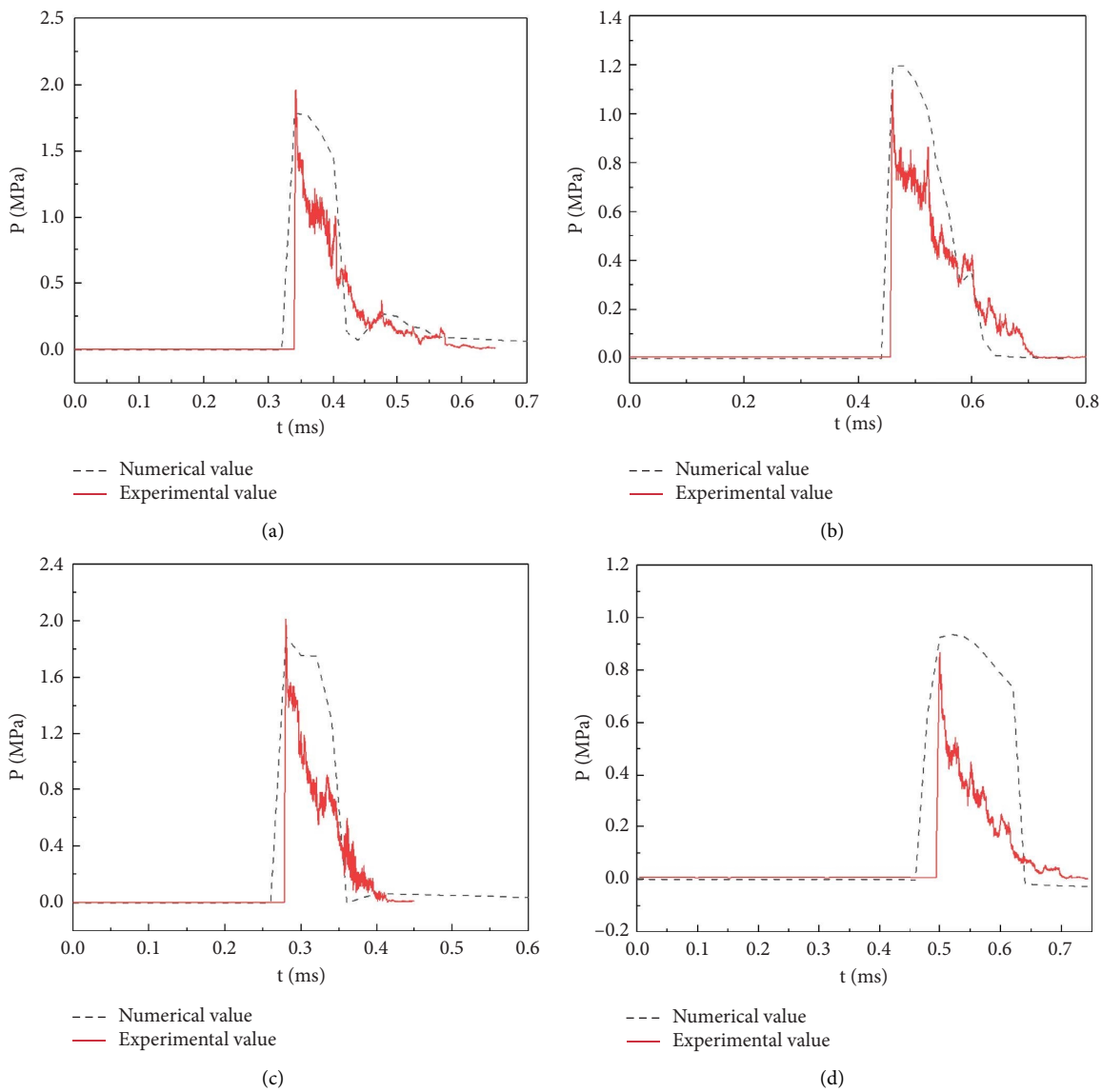

Figure 10: Pressure curve at monitoring points with device.

Table 2: Peak pressure at the monitoring points with device.

Serial number	Numerical value (MPa)	Experimental value (MPa)	Error (%)
1	1.78	1.96	9.2
2	1.20	1.11	8.1
3	1.89	2.01	6.0
4	0.94	0.86	9.3

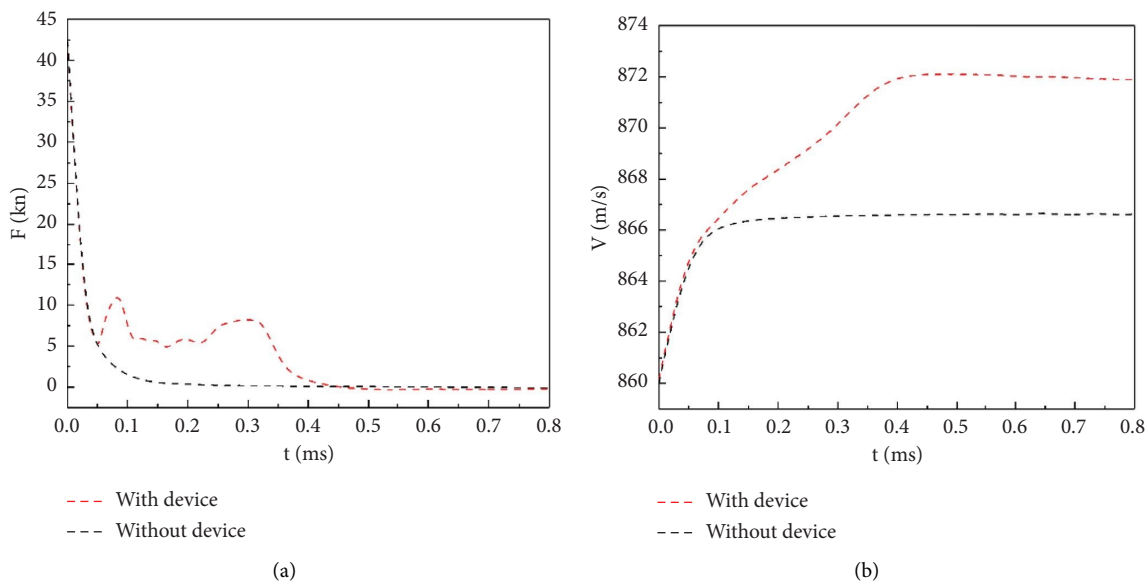

Figure 11: Process of the changing projectile motion state. (a) Axial force on the projectile. (b) Projectile velocity.

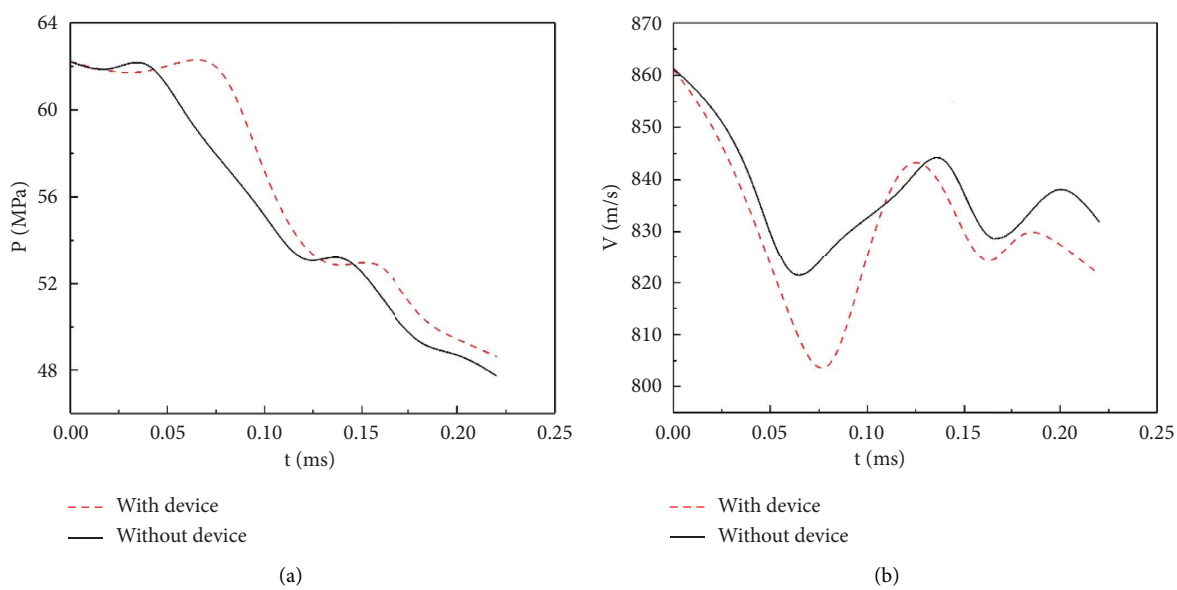

Figure 12: Gas parameters at the center of the muzzle. (a) Pressure. (b) Velocity.

4. Conclusions

Based on Euler equations, the hybrid Roe type scheme and the structured dynamic overlapping grid technique are employed to investigate the formation and development of complex flow field structure in the firing process of aircraft gun. The muzzle flow field is simulated under two conditions, without muzzle decompression device and with muzzle decompression device. For muzzle decompression devices, the formation of the precursor shock wave is more complicated, and multiple shock waves are generated during the expansion of propellant gas in the center hole of the device.

Based on the three-dimensional solution of the launch process with a muzzle decompression device and the two-dimensional axisymmetrical solution of the launch process without a muzzle decompression device, the decompression efficiency of the device can reach 40% at some characteristic points, which agrees well with the corresponding experimental

result. The results show that the numerical calculation method can be used as guidance for the design and development of muzzle decompression device.

Data Availability

All data generated or analyzed during this study are included within the article.

Conflicts of Interest

The authors declare that they have no conflicts of interest.

Acknowledgments

This work was supported by the Foundation Enhancement Program of China (no. 2019xxxx315).

References

[1] X. H. Jiang, Z. H. Chen, B. C. Fan, and H. Z. Li, "Numerical simulation of blast flow fields induced by a high-speed projectile," *Shock Waves*, vol. 18, no. 3, pp. 205–212, 2008.

[2] A. Merlen, "Generalization of the muzzle wave similarity rules," *Shock Waves*, vol. 9, no. 5, pp. 341–352, 1999.

[3] Z. L. Jiang, "Wave dynamic processes induced by a supersonic projectile discharging from a shock tube," *Physics of Fluids*, vol. 15, no. 6, pp. 1665–1675, 2003.

[4] Z. J. Li, H. Wang, C. S. Chen, and H. X. Huang, "Effects of different constrained boundary structures on the evolution of shock waves and vortexes in muzzle jets," *Journal of Mechanical Science and Technology*, vol. 37, no. 10, pp. 5239–5249, 2023.

[5] Z. J. Li and H. Wang, "Evolution of shock waves during muzzle jet impinging moving bodies under different constrained boundaries," *Aerospace*, vol. 10, no. 11, p. 908, 2023.

[6] B. Zhang, H. Liu, F. Chen, and G. Wang, "Numerical simulation of flow fields induced by a supersonic projectile moving in tubes," *Shock Waves*, vol. 22, no. 5, pp. 417–425, 2012.

[7] Z. Li and H. Wang, "Influence of different velocities on muzzle flow field," *Transactions of Nan Jing University of Aeronautics and Astronautics*, vol. 36, no. 1, pp. 88–97, 2019.

[8] Z. Q. Sun, Q. Li, P. Qu, and L. Lu, "Numerical investigation of the influence of supersonic flow on muzzle combustion," *Physics of Fluids*, vol. 35, no. 2, 2023.

[9] Z. Q. Sun, Q. Li, and P. Qu, "Numerical investigation of the influence of supersonic flow on muzzle combustion," *Physics of Fluids*, vol. 35, no. 2, 2023.

[10] X. C. Xue and Y. G. Yu, "Investigation of thermal performance in dual-fuel units," *Energy Science and Engineering*, vol. 10, no. 12, pp. 4782–4803, 2022.

[11] P. F. Li and X. B. Zhang, "Numerical research on adverse effect of muzzle flow formed by muzzle brake considering secondary combustion," *Defence Technology*, vol. 17, no. 4, pp. 1178–1189, 2021.

[12] D. Wang, F. Nan, X. Liao, Z. Xiao, P. Du, and B. Wang, "Characteristics of muzzle flow field of large caliber gun considering chemical reaction," *Acta Armamentarii*, vol. 42, no. 8, pp. 1624–1630, 2021.

[13] D. Wang, F. Nan, X. Liao, Z. Xiao, P. Du, and B. Wang, "Effect of flame inhibitor of the muzzle flame of large caliber gun," *Acta Armamentarii*, vol. 43, no. 2, pp. 273–278, 2022.

[14] A. Moumen, B. Stirbu, J. Grossen, D. Laboureur, J. Gallant, and P. Hendrick, "Particle image velocimetry for velocity measurement of muzzle flow: detailed experimental study," *Powder Technology*, vol. 405, Article ID 117509, 2022.

[15] A. Moumen, J. Grossen, I. Ndindabahizi, J. Gallant, and P. Hendrick, "Visualization and analysis of muzzle flow fields using the Background-Oriented Schlieren technique," *Journal of Visualization*, vol. 23, no. 3, pp. 409–423, 2020.

[16] X. F. Kong, L. Q. Wang, T. Yu, Z. He, H. Luo, and B. M. Li, "Free-field shock-wave test method for meteorological air cannons," *Measurement*, vol. 189, Article ID 110456, 2022.

[17] C. Qiankun, L. Panfei, Z. Qi, W. Xuefeng, and L. Meng, "Research on the measurement of muzzle shock wave pressure field for a naval gun," *IOP Conference Series: Earth and Environmental Science*, vol. 791, no. 1, Article ID 012096, 2021.

[18] X. Y. Zhao, K. D. Zhou, L. He, Y. Lu, J. Wang, and Q. Zheng, "Numerical simulation and experiment on impulse noise in a small caliber rifle with muzzle brake," *Shock and Vibration*, vol. 2019, Article ID 5938034, 12 pages, 2019.

[19] Z. H. Ding and K. Wang, "Iop in Fatigue life prediction of aircraft gun cabin structure under impact," in *Proceedings of the 13th Asia Conference on Mechanical and Aerospace Engineering (ACMAE), Chengdu, Peoples R China*, PEOPLES R CHINA, Chengdu, China, December 2022.